Band structure of wurtzite GaBiAs nanowires

Bin Zhang, Yuqing Huang, Jan Eric Stehr, P.P. Chen, X. J. Wang, W Lu, Weimin Chen and Irina A Buyanova

The self-archived postprint version of this journal article is available at Linköping University Institutional Repository (DiVA):
http://urn.kb.se/resolve?urn=urn:nbn:se:liu:diva-160735

N.B.: When citing this work, cite the original publication.
Zhang, B., Huang, Y., Stehr, J. E., Chen, P., Wang, X. J., Lu, W, Chen, W., Buyanova, I. A, (2019), Band structure of wurtzite GaBiAs nanowires, *Nano letters (Print)*, 19, 6454-6460.
https://doi.org/10.1021/acs.nanolett.9b02679

Original publication available at:
https://doi.org/10.1021/acs.nanolett.9b02679

Copyright: American Chemical Society
http://pubs.acs.org/

LINKÖPING UNIVERSITY

Band structure of wurtzite GaBiAs nanowires

Bin Zhang†, ‡, Yuqing Huang†, Jan Eric Stehr†, Ping-Ping Chen‡, Xing-Jun Wang, ‡, W. Lu‡, Weimin M. Chen† and Irina A. Buyanova**, †*

† Department of Physics, Chemistry and Biology, Linköping University, S-581 83 Linköping, Sweden

‡ State Key Laboratory of Infrared Physics, Shanghai Institute of Technical Physics, Chinese Academy of Sciences, Shanghai 200083, China

KEYWORDS

Wurtzite, nanowire, GaBiAs, photoluminescence, photoluminescence excitation, resonant Raman, band structure

ABSTRACT

We report on the first successful growth of wurtzite (WZ) GaBiAs nanowires (NWs) and reveal effects of Bi incorporation on electronic band structure by using polarization-resolved optical spectroscopies performed on individual NWs. Experimental evidence of a decrease of the band-gap energy and an upward shift of the topmost three valence subbands upon incorporation of Bi atoms is provided, whereas the symmetry and ordering of the valence band states remain unchanged, that is, Γ_9, Γ_7 and Γ_7 within the current range of Bi compositions. The extraordinary valence band structure of wurtzite GaBiAs NWs is explained by anisotropic hybridization and anti-crossing between p-like Bi states and extended valence band states of host WZ GaAs. Moreover, incorporation of Bi into GaAs is found to significantly reduce temperature sensitivity of the band-gap energy in WZ GaBiAs NWs. Our work therefore demonstrates that utilizing dilute bismide alloys provides new avenues for band-gap engineering and thus photonic engineering with NWs.

One-dimensional semiconductor nanowires (NWs) based on III-V semiconductors, such as GaAs and related alloys, have gained a considerable research interest owing to their potential for future optoelectronic and photonic applications.[1, 2] Indeed, the unique one-dimensional architecture and a large dielectric mismatch between the NW and its surrounding render its strong optical anisotropy[3], which by coupling with selection rules of inter-band optical transitions leads to intriguing polarization properties of photodetection and light emission.[4, 5] For example, photoluminescence (PL) emission from GaAs-based NWs with zinc-blende (ZB) structure typically exhibits strong linear polarization parallel to the NW axis.[6] However, the PL polarization direction can be switched to the perpendicular one in GaNAs NWs with only 0.5% of nitrogen, owing to the N-induced formation of self-aligned quantum dots.[7] Moreover, the NW geometry enables material crystallization with new lattice structures, such as wurtzite (WZ) crystal phase in GaAs and InP-based materials[8, 9] that otherwise only crystalize as ZB in bulk crystals and thin film. Changes in the crystal structure are expected to affect physical properties, which opens unprecedented possibilities to engineer electronic properties and also polarization of light absorption and emission through fabrication of mixed-phase heterostructures along the axis or radius of NWs.[10]

Among GaAs-based semiconductors, highly mismatched alloys have been extensively researched owing to their unusual fundamental physical properties attractive for applications in photonics and optoelectronics. One of the promising candidates for these potential applications is GaBiAs alloy. Previous studies of GaBiAs epilayers have shown that an addition of a dilute concentration of bismuth (Bi) into ZB GaAs causes a strong perturbation of valence band (VB) states leading to a giant reduction of the band-gap energy (E_g). For example, incorporating only 1% of Bi into GaAs induces a large reduction of ~90 meV in the band-gap energy. [11, 12] Therefore, by carefully adjusting the Bi composition in Ga(In)As(N), the emission energy can be tuned to cover the fiber-optic communication windows at 1.3 μm and 1.55 μm. Furthermore,

since Bi is a heavy element, alloying with it causes a strong increase of the spin-orbit (SO) interaction and the SO splitting energy (Δ_{SO}). In the alloys with a sufficiently high Bi content the condition of $E_g < \Delta_{SO}$ helps to suppress non-radiative Auger recombination losses and inter-valence band absorption[13-16], which is favorable for optimization of threshold current and quantum efficiency of near-infrared lasers.[17] Additional benefits of using these highly mismatched alloys in optoelectronic structures include reduced temperature sensitivity of the band-gap energy upon Bi incorporation. [18, 19] The increased SO interaction and the possibility to fine-tune it by small changes in the Bi content may prove useful for spintronic devices. [20, 21]

Unfortunately, synthesis of GaBiAs in the NW geometry remains highly challenging, impeding full exploitation of the benefits provided by this architecture. Lu *et al.* [22] observed that presence of Bi during the NW growth favors the formation of ZB crystal structure in GaAs NWs, indicating impactful power of Bi in engineering the crystal structure. However, due to a relatively high growth temperature Bi atoms acted as bonding antisurfactant on the GaAs surface and did not participate in the alloy formation. Recently, several groups[23, 24] have succeeded to grow metamorphic GaBiAs NWs, all of which exhibited predominantly the ZB structure with a high degree of polymorphisms. A decrease in the band-gap energy upon Bi incorporation was observed, similar to the case of GaBiAs epilayers. On the other hand, fabrication of GaBiAs with WZ structure was not achieved so far and its electronic properties remain completely unknown.

In this work, we report on the first successful growth of WZ GaBiAs NWs with high optical quality and evaluate the band structure of WZ GaBiAs, by employing polarization-resolved PL, PL excitation (PLE) and resonant Raman measurements performed on individual NWs, combined with the high-resolution transmission electron microscopy (TEM). We show that alloying with Bi reduces the band-gap energy of WZ GaBiAs and largely affects splitting between the VB subbands, which experience a significant upward shift relative to their energy

positions in parental WZ GaAs. These findings are explained by anisotropic hybridization between p-like Bi states and extended VB states of host WZ GaAs by expanding valence-band anticrossing (VBAC) theory.

The investigated GaBiAs NWs were grown on (111)-B GaAs substrates by Au-assisted molecular beam epitaxy (MBE) via a vapor-liquid-solid (VLS) mechanism. (See Methods for a more detailed description of the NW growth). As a reference, we also fabricated pure GaAs NWs grown under the same conditions as the GaBiAs NWs but without a Bi source. All NWs are found to be tapered with their diameter varying from about 33-43 nm at the NW top to 70-120 nm at the bottom. Structural differences between the GaBiAs and GaAs nanowires were evaluated by TEM. Representative TEM micrographs of GaBiAs (a) and GaAs (b) NWs are shown in Figure 1. The GaAs NWs predominantly crystalized in the WZ structure marked by the green line in Figure 1 (b) with a 2H stacking sequence (ABAB). To make clear the crystal phase of nanowires, the insets depict high-resolution TEM (HR-TEM) images together with fast Fourier transform (FFT) patterns of the bottom part (left-hand side) and top part (right-hand side) of the GaAs NW. The GaBiAs NWs also crystalized in the WZ (2H) structure within the bottom half of the NW with the length of about 1.2-1.5 μm (marked by the green line in Figure 1 (a)). In the upper half of the NWs (marked by the red line) the crystal structure is predominantly transformed to the 4H polytype with an ABAC stacking sequence. The transformation of the crystal structure in the GaBiAs NW can be seen in the FFT patterns of the lower and upper half of the GaBiAs NW. For NWs grown under identical growth conditions, the transformation from WZ (2H) to 4H polytype is commonly observed in the middle of the NWs as depicted in Figure 1. Structural defects in the form of randomly nucleated stacking faults formed perpendicular to the NW growth axis can be observed over the entire length of both GaAs and GaBiAs NW. The appearance of the stacking faults is probably due to a high V/III flux ratio used in the growth process.[25, 26]

From Fig.1, it is obvious that GaAs and GaBiAs NWs have the same hexagonal 2H WZ structure at the bottom part of the NWs. This allowed us to evaluate the participation of Bi in the alloy formation and its effects on the electronic structure of WZ GaAs. For these purposes, polarization-resolved μ-PL measurements were implemented on individual GaAs and GaBiAs NWs that were mechanically transferred on a Si substrate. In all cases the excitation light was focused on the thick bottom region of the NWs. Considering that the excitation spot had a smaller diameter (around 0.8 μm) than the length of WZ segments (1.3-1.5 μm in the GaBiAs NWs), this ensured that the optical properties were probed exclusively from the 2H WZ regions. A schematic diagram of the measurement configuration is shown in Figure 2(a). The Cartesian coordinate system is set with the z-axis along the NW growth direction coinciding with the crystallographic c-axis, while the x-axis is parallel to the direction of the incoming laser excitation and back-detection light, that is, the crystallographic $[11\bar{2}0]$ direction. Typical low-temperature (T=5K) μ-PL spectra measured from single GaAs and GaBiAs NWs are displayed in Figure 2 (c) and (d), respectively. The dominant emission peak at 1.516 eV detected from the GaAs NW corresponds to the free exciton emission in WZ GaAs.[9, 27] A weak shoulder at slightly lower energies is likely associated with stacking faults or unintentional dopants.[28] In contrast to the GaAs NW, the PL emission band of the GaBiAs NW exhibits a considerable redshift of ~28 meV and is markedly broadened, as shown in Figure 2 (d). This indicates Bi incorporation in the NW and the formation of WZ GaBiAs alloy. The red shift of the PL emission represents combined effects of the Bi-induced band-gap reduction and exciton localization within the band-tail states. The latter also causes broadening of the PL spectra as was extensively documented in planar ZB GaBiAs alloys. [29]

The PL emissions from both GaBiAs and GaAs NWs are found to be linearly polarized in the direction perpendicular to the NWs axis - see Figure 2 (c) and (d) and also Supporting information. Such PL polarization is typical for WZ GaAs [30], where conduction band (CB)

states have Γ_7 symmetry, whereas combined effects of crystal field and SO interactions split the VB states into the so-called A-, B- and C-subbands with Γ_9, Γ_7 and Γ_7 symmetry, respectively – see Figure 2(b). Radiative recombination between Γ_7 electrons and Γ_9 heavy holes (HH) is only dipole-allowed when the electric field vector (E) is perpendicular to the crystallographic c-axis that coincides with the NW axis. This means that linear polarization of -100% is expected according to the optical selection rules. (Here the degree of linear polarization is defined as $P = (I_{\parallel} - I_{\perp}) / (I_{\parallel} + I_{\perp}) \times 100\%$, where $I_{\parallel}$ ($I_{\perp}$) is the intensity of the PL component that is linearly polarized parallel (perpendicular) to the NW axis). However, the existing dielectric contrast between thin NWs and their surroundings will further modulate the emission polarization, by substantially weakening the emitted light that is polarized perpendicular to the NW axis without affecting the emission component with parallel polarization.[3] A typical degree of linear PL polarization measured in the GaBiAs NW is -33%. By applying the so-called antenna theory to filter-out the above-mentioned effect of the dielectric mismatch,[4] the PL polarization inside the GaBiAs NW is estimated to be as high as -97% (see Supporting information). This result unambiguously shows that the topmost VB of the investigated GaBiAs NWs have the same Γ_9 symmetry as that in WZ GaAs.

According to the previous studies of planar GaBiAs alloy,[11, 31, 32] adding dilute concentrations of Bi atoms into ZB GaAs substantially modifies the valence band structure, whereas CB states remain largely unperturbed. To further explore the VB structure of WZ GaBiAs, polarization-resolved μ-PLE spectra were measured from individual GaBiAs NWs and the corresponding results are presented on the right side of Figure 2 (d). For comparison, the μ-PLE spectra of the reference GaAs NW are also shown – see the right panel of Figure 2(c). In both cases the detection energy was fixed at the peak energy of the PL emission, as marked by the vertical dashed lines. As the excitation laser energy is scanned to higher energies, a clear onset in the PLE intensity is observed for both nanowires. Since the PLE spectra to some

extent are equivalent to absorption spectra, any enhancement of light absorption due to optical transitions involving higher-energy valence subbands should increase the PL intensity. Therefore, we ascribe the step-like increase in the PLE intensity to the onset of optical absorption transitions between the light hole (LH)-like B- valence subband and CB. The corresponding energy in the GaAs NW (E_B^{GaAs}) is 1.618 eV, consistent with the reported value of 1.62 eV by resonant Raman scattering experiments.[27, 33] It is noticeable that it is shifted to a significantly lower value of E_B^{GaBiAs} =1.581 eV in the GaBiAs NWs. (The E_B^{GaAs} and E_B^{GaBiAs} values were determined by linearly extrapolating the corresponding spectral dependences of the squared PL intensity, I_{PL}^2). Since the PLE technique is generally not sensitive to localized states, which shows that Bi incorporation leads to an upward shift of the B VB-subband by about 37 meV. Moreover, the PLE intensity above the B-absorption edge for both NWs is significantly stronger when the excitation light is linearly polarized parallel to the crystallographic c-axis, which is opposite to the polarization of the PL spectra. This is because the $\Gamma_7(B) - \Gamma_7(CB)$ transitions are dipole allowed for both $E \perp c$ and $E \parallel c,$ as shown in Figure 2 (b). The latter polarization is further enhanced by the antenna effect leading to the overall $E \parallel c$ polarization of the $\Gamma_7(B) - \Gamma_7(CB)$ transitions in the PLE spectra. The detected parallel polarization of the PLE spectra in the GaBiAs NWs, therefore, suggests that B- valence subband in WZ GaBiAs has Γ_7 symmetry.

The limited spectral range of the excitation laser used in the PLE measurements prevents using this technique for determining the energy position of the higher-lying C- valence subband. Therefore, to ascertain the effect of Bi incorporation on these states we employed resonant Raman scattering. This technique allows to observe forbidden longitudinal optical (LO) phonon scattering under resonant conditions, that is, when the energy of either incident laser photon ($\hbar\omega_i$) or scattered photon ($\hbar\omega_s$) coincides with the energy of a real state in a semiconductor, owing to the electron-phonon interaction via the dipole-forbidden Fröhlich coupling

mechanism.[34, 35] Under a fixed excitation wavelength (660 nm in our measurements) the resonant conditions can be reached by varying sample temperature (T), which causes a shift of the $\Gamma_7(C) - \Gamma_7(CB)$ transition energy (E_C), as shown schematically in Figure 3(a). A typical Raman spectrum measured at 300K from a GaBiAs NW is shown in the inset in Figure 3(b) and is dominated by the scattering peak involving zone-center transverse optical (TO) phonons (see also Supporting information). The LO Raman mode is weak, as expected from the Raman selection rules in the measurement geometry. The LO intensity, however, is substantially enhanced with decreasing T and reaches its maximum value at T= 90 K. This can be seen from Figure 3(b) which shows temperature dependence of the I_{LO}/I_{TO} ratio (circles), where I_{LO} (I_{TO}) denotes the intensity of the LO (TO) mode. The resonant profile of LO scattering can be fit by a Gaussian function (the solid line) and shows a single outgoing resonance, as was also observed previously in GaAs NWs.[36] In contrast, the LO scattering intensity in the GaAs NWs remains at a relatively low level (see Fig. 3(b), squares) within the whole temperature range. This is expected as the $\Gamma_7(C) - \Gamma_7(CB)$ transition energy (E_C^{GaAs}) of WZ GaAs remains beyond the resonance conditions (~1.868 eV at T=300K) as schematically illustrated in Figure 3 (a).[36] At the resonant temperature, the $\Gamma_7(C) - \Gamma_7(CB)$ transition energy E_C^{GaBiAs} of WZ GaBiAs can then be determined as:

$$E_C^{GaBiAs} = \hbar\omega_i - \hbar\omega_{LO} \qquad (1)$$

where $\hbar\omega_i$ corresponds to the excitation laser energy of 1.88 eV and $\hbar\omega_{LO}$ is the LO phonon energy of 36.5 meV. This yields E_C^{GaBiAs} =1.844 eV at T=90K, which is about 122 meV lower than that in WZ GaAs, that is, 1.966eV at T=90 K.[36] We note that this change of the transition energy is much larger than that for the $\Gamma_7(B) - \Gamma_7(CB)$ and $\Gamma_9(A) - \Gamma_7(CB)$ transitions, which means that the splitting between the A/B and C valence subbands is reduced upon Bi incorporation.

The observed transformation of the electronic structure of GaBiAs NWs is unlikely related to strain effects caused by Bi incorporation, as the investigated NWs have uniform structure without core/shell layers and also without polymorphism within the investigated region (i.e. the bottom segment of NWs), as revealed by the HRTEM characterization (see figure 1). This conclusion is further supported by the performed Raman measurements that show the same positions of Raman peaks in both GaBiAs NWs and reference GaAs NWs (see Supporting information). To understand the origin of the observed Bi-induced changes of the VB states, we first briefly recall the effects of Bi incorporation on the VB structure of the ZB polytype. When Bi replaces a group-V element, it introduces p-like localized states that are resonant with VB and have basis functions identical to those describing VB states of the host semiconductor[31, 37, 38]. The topmost Bi level E_{Bi} at E_v - 0.4 eV is formed from the HH- and LH-VB states, whereas the much deeper E_{Bi-SO} level at E_v-1.9 eV is mainly derived from the SO-split VB states[31] – see the left panel of Figure 4(a). The anticrossing interaction between these Bi-related states and extended VB states of the same character causes splitting of the VB states and a strong upward shift of the VB edge leading to the giant bowing in the band-gap energy and an increase in Δ_{SO}.[11, 31] These modifications of the VB can be accurately described by the so-called VB anticrossing (VBAC) model assuming a single isotropic coupling parameter between the Bi states and VB states.[31]

In principle, a similar description should be applicable to WZ GaAs. Assuming that the localized defect level is constant relative to the vacuum level and applying the valence band offset of 0.076 eV between ZB and WZ GaAs,[39] the E_{Bi} and E_{Bi-SO} in WZ GaAs are estimated to be at E_v -0.476 eV and E_v-1.976 eV, respectively. Similar to the VB states, the WZ crystal field may further split the E_{Bi} level into the HH-like and LH-like states with Γ_9 and Γ_7 symmetry, respectively. Although the crystal field also mixes the LH states with SO split-off states with Γ_7 symmetry, this mixing of states is rather minor due to the large energy separation

between these two interacting states. [40, 41] In the spirit of the VBAC theory,[31] the heavy (light) hole states of the host matrix, that is, A(B) valence subband, only interact with heavy (light) hole states of Bi. On the contrary, the C subband experiences anticrossing with the E_{Bi-SO} level. The interaction strength critically depends on the energy distance between the interacting states, increasing for the states that are close in energy. The energy difference between the E_{Bi-SO} level and C valence subband of GaAs is about ~1.51 eV, whereas that between E_{Bi} and B valence subband is only ~0.376 eV. Therefore, the upward shift of the C valence subband should be smaller than that of the B- (and A-) valence subbands if the interaction parameter is isotropic; namely it is the same for all interacting states. This is in obvious disagreement with our experimental results.

The fact that the upward shift of the C valence subband in GaBiAs exceeds that of the A and B VB subbands means that the former experiences stronger anticrossing repulsion with the Bi-related localized states. This in turn implies that the hybridization energy between the localized Bi states and orbital host states is anisotropic near the center of Brillouin zone, as is in principle required from the symmetry of hexagonal WZ crystals, that is,

$$V_{X,Y} = \langle P_X^{Bi}|U|X\rangle = \langle P_Y^{Bi}|U|Y\rangle = C_{X,Y}\sqrt{x},\ V_Z = \langle P_Z^{Bi}|U|Z\rangle = C_Z\sqrt{x} \qquad (2).$$

Here U denotes the localized potential of Bi in the host matrix, $P_{X,Y,Z}^{Bi}$ refers to the wave function of Bi, and X (Y, Z) is the orbital states of the host. Diagonalizing the 12×12 matrix Hamiltonian yields six doubly degenerate eigenvalues (see Supporting information), which correspond to restructured valence band states in WZ GaBiAs as depicted in Figure 4(b) where the vertical arrows denote the interacting states with the specified hybridization energies. The best agreement between the simulation and experimental data is obtained by setting the hybridization energy $V_{X,Y} = 0.0947\ eV$ and $V_Z = -0.2407\ eV$. If we assume that the coupling parameter $C_{X,Y}$ has the same value as that of planar GaAs, that is, 1.55 eV, the other coupling parameter C_Z and Bi concentration x can then be estimated as -3.94 eV and 0.004, respectively.

Figure 4(b) displays the simulated valence band structure as a function of hybridization energy $V_{X,Y}$. The simulations also predict that the ordering between the A(Γ_9) and B(Γ_7) VB states can be reversed in WZ GaBiAs with high Bi compositions. This will further extend flexibility in band structure engineering allowing us, for example, to achieve parallel polarization of the emitted light in thin WZ NWs.

In addition to the modifications of the band structure, Bi incorporation in ZB GaAs was found to slow down temperature dependence of its bandgap.[19] In order to check whether this remains true in the WZ polytype, we have performed temperature-dependent PL measurements. The maximum position of the PL emission in the GaBiAs NWs is found to exhibit the so-called "S-shape" dependence – see Figure 5, the red filled circles. Such dependence is typical for highly mismatched alloys[42, 43], including ZB GaBiAs[29], where the initial blue shift reflects thermal activation of the excitons from the localized to extended states whereas the subsequent red shift at higher temperatures is due to a reduction of the band-gap energy. Consistently, only a red shift of the PL emission that is not prone to localization effects is observed in the reference GaAs NWs (see Figure 5, the blue squares). The PL peak positions in the GaAs and GaBiAs NW could be fitted (the solid lines in Fig.5) with an extended version of the Varshni's equation.[44]

$$E_g(T) = E_g(0) - \frac{\alpha T^4}{\beta + T^3} \quad (3)$$

where α and β are the material related parameters. Noticeably, the bandgap of GaBiAs NW exhibits a remarkable reduction of temperature sensitivity with $\alpha = 0.209$ meV/K that is much smaller than $\alpha = 0.241$ meV/K in WZ GaAs. Considering that dilute concentration of Bi mainly affects the valence band, the decrease of temperature sensitivity in GaBiAs can be attributed to an increased localized character of the VB edge, consistent with the previous observation in planar ZB GaBiAs.[19]

In summary, we have successfully fabricated WZ GaBiAs NWs with good optical quality. The electronic band structure of wurtzite GaBiAs NW was revealed by employing spatially resolved optical spectroscopies on individual NWs. The band-gap energy of WZ GaBiAs is reduced as compared with parental GaAs. The polarization-resolved μ-PL and μ-PLE spectra indicate that both the A and B valence subbands of the WZ GaAs NW are pushed upwards by anticrossing repulsion following incorporation of Bi atoms, while the symmetry order of the VB states is kept unchanged under the current Bi compositions. Surprisingly, the shift is even larger for the C valence subband based on the performed resonant Raman measurement, which is unexpected considering the large energy distance between the C subband and the SO-split Bi level. The extraordinary modifications of the VB states are interpreted by expanding the VBAC model and assuming anisotropic hybridization energy in wurtzite GaBiAs NW. The model also predicts that the ordering of the A and B VB states can be switched in WZ GaBiAs alloys with larger Bi compositions, which could allow control of polarization direction of emitted and absorbed light in thin WZ NWs via alloying. Furthermore, incorporation of Bi into GaAs significantly reduces the temperature sensitivity of the band gap in WZ GaBiAs NW. Our work therefore demonstrates that utilizing dilute bismide alloys provides new avenues for band-gap engineering and thus photonic engineering with NWs.

Methods

The Ga(Bi)As NWs studied in this work were grown on GaAs(111)B substrates by Au-assisted MBE via the VLS mechanism. The substrate temperature was set to ~353℃, given the fact that a lower growth temperature is advantageous for Bi incorporation.[45] During the growth

of GaBiAs NWs, the As_4/Ga beam equivalent pressure (BEP) ratio was ~30 and a Bi source shutter was opened for 30 min to supply a Bi flux of 8.6×10^{-8} Torr. Then, the Bi source was closed for 1 min to finish growth. For comparison, pure GaAs NWs were also grown at the same conditions, but with the Bi shutter closed during the entire growth process. An FEI Tecnai G2 TF 20 UT transmission electron microscope was used to study the crystal structure of individual nanowires that were mechanically transferred to a carbon/copper TEM grid.

For optical characterization, NWs were mechanically transferred to gold-coated SiO_2 substrates. All optical measurements were carried out using a confocal Horiba Jobin-Yvon HR800 system. A solid-state 660-nm laser was used for Resonant Raman scattering measurements and an excitation power below 1 mW/μm^2 was chosen to avoid heating effects. The induced Raman scattering signal was collected with a long focal length objective (50×, NA=0.5) in a back-scattering configuration, dispersed by a grating monochromator and detected with a cooled charge-coupled-device detector. For low-temperature optical measurements, the samples were mounted in a He(N_2)-flow cryostat. The polarization-resolved PL signal was analyzed using a half-wave plate coupled with a fixed linear polarizer. The polarization-resolved PLE measurements were performed using a tunable Ti:Sapphire laser. During the PLE measurements, a beam splitter and a power-meter were used to synchronously record and calibrate the incident excitation intensity at each wavelength.

ASSOCIATED CONTENT

Supporting Information.

PL Polarization inside GaBiAs nanowires, temperature dependent Raman spectra of Ga(Bi)As nanowires, VBAC modelling. This material is available free of charge via the Internet at http://pubs.acs.org

AUTHOR INFORMATION

Corresponding Author

*E-mail: xjwang@mail.sitp.ac.cn

**E-mail: irina.bouianova@liu.se

Notes

The authors declare no competing financial interest.

ACKNOWLEDGMENT

Financial support by Linköping University through the Professor Contracts, the Swedish Research Council (Grant No. 2016-05091), the Swedish Energy Agency (Grant No. P40119-1), the Swedish Government Strategic Research Area in Materials Science on Functional Materials at Linköping University (Faculty Grant SFO-Mat-LiU No 2009 00971), the National Natural Science Foundation of China (Grant Nos. 11874377), Natural Science Foundation of Shanghai (Grant No. 18ZR1445700) and Shanghai Science and Technology Foundation (Grant Nos. 18JC1420401) are greatly appreciated. B. Zhang acknowledges the support from China Scholarship Council (No. 201604910582).

REFERENCES

(1) Joyce, H. J.; Gao, Q.; Hoe Tan, H.; Jagadish, C.; Kim, Y.; Zou, J.; Smith, L. M.; Jackson, H. E.; Yarrison-Rice, J. M.; Parkinson, P.; Johnston, M. B. *Prog. Quantum Electron.* **2011,** 35, (2-3), 23-75.

(2) Chen, S.; Jansson, M.; Stehr, J. E.; Huang, Y.; Ishikawa, F.; Chen, W. M.; Buyanova, I. A. *Nano Lett.* **2017,** 17, (3), 1775-1781.

(3) Ruda, H. E.; Shik, A. *Phys. Rev. B* **2005,** 72, (11), 115308.

(4) Filippov, S.; Sukrittanon, S.; Kuang, Y.; Tu, C.; Persson, P. O.; Chen, W. M.; Buyanova, I. A. *Nano Lett.* **2014,** 14, (9), 5264-9.

(5) De Luca, M.; Polimeni, A. *Appl. Phys. Rev.* **2017,** 4, (4), 041102.

(6) Titova, L. V.; Hoang, T. B.; Jackson, H. E.; Smith, L. M.; Yarrison-Rice, J. M.; Kim, Y.; Joyce, H. J.; Tan, H. H.; Jagadish, C. *Appl. Phys. Lett.* **2006,** 89, (17), 173126.

(7) Filippov, S.; Jansson, M.; Stehr, J. E.; Palisaitis, J.; Persson, P. O.; Ishikawa, F.; Chen, W. M.; Buyanova, I. A. *Nanoscale* **2016,** 8, (35), 15939-47.

(8) Zardo, I.; Conesa-Boj, S.; Peiro, F.; Morante, J. R.; Arbiol, J.; Uccelli, E.; Abstreiter, G.; Fontcuberta i Morral, A. *Phys. Rev. B* **2009,** 80, (24), 245324.

(9) Ahtapodov, L.; Todorovic, J.; Olk, P.; Mjaland, T.; Slattnes, P.; Dheeraj, D. L.; van Helvoort, A. T.; Fimland, B. O.; Weman, H. *Nano Lett.* **2012,** 12, (12), 6090-5.

(10) Ba Hoang, T.; Moses, A. F.; Ahtapodov, L.; Zhou, H.; Dheeraj, D. L.; van Helvoort, A. T.; Fimland, B. O.; Weman, H. *Nano Lett.* **2010,** 10, (8), 2927-33.

(11) Alberi, K.; Dubon, O. D.; Walukiewicz, W.; Yu, K. M.; Bertulis, K.; Krotkus, A. *Appl. Phys. Lett.* **2007,** 91, (5), 051909.

(12) Francoeur, S.; Seong, M. J.; Mascarenhas, A.; Tixier, S.; Adamcyk, M.; Tiedje, T. *Appl. Phys. Lett.* **2003,** 82, (22), 3874-3876.

(13) Sweeney, S. J.; Jin, S. R. *J. Appl. Phys.* **2013,** 113, (4), 043110.

(14) Usman, M.; Broderick, C. A.; Lindsay, A.; O'Reilly, E. P. *Phys. Rev. B* **2011,** 84, (24), 245202.

(15) Wu, X.; Pan, W.; Zhang, Z.; Li, Y.; Cao, C.; Liu, J.; Zhang, L.; Song, Y.; Ou, H.; Wang, S. *ACS Photonics* **2017,** 4, (6), 1322-1326.

(16) Marko, I. P.; Broderick, C. A.; Jin, S.; Ludewig, P.; Stolz, W.; Volz, K.; Rorison, J. M.; O'Reilly, E. P.; Sweeney, S. J. *Sci Rep* **2016,** 6, 28863.

(17) Allam, J. *High pressure in semiconductor physics II* **1998,** 55, 301.

(18) Yoshida, J.; Kita, T.; Wada, O.; Oe, K. *Jpn. J. Appl. Phys.* **2003,** 42, (2a), 371-374.

(19) Pettinari, G.; Capizzi, M.; Polimeni, A. *Semicond. Sci. Technol.* **2015,** 30, (9), 094002.

(20) Bychkov, Y. A.; Rashba, E. I. *J. Phys. C: Solid State Phys.* **1984,** 17, (33), 6039-6045.

(21) Kato, Y. K.; Myers, R. C.; Gossard, A. C.; Awschalom, D. D. *Science* **2004,** 306, (5703), 1910-3.

(22) Lu, Z.; Zhang, Z.; Chen, P.; Shi, S.; Yao, L.; Zhou, C.; Zhou, X.; Zou, J.; Lu, W. *Appl. Phys. Lett.* **2014,** 105, (16), 162102.

(23) Ishikawa, F.; Akamatsu, Y.; Watanabe, K.; Uesugi, F.; Asahina, S.; Jahn, U.; Shimomura, S. *Nano Lett.* **2015,** 15, (11), 7265-72.

(24) Zelewski, S. J.; Kopaczek, J.; Linhart, W. M.; Ishikawa, F.; Shimomura, S.; Kudrawiec, R. *Appl. Phys. Lett.* **2016,** 109, (18), 182106.

(25) Joyce, H. J.; Wong-Leung, J.; Gao, Q.; Tan, H. H.; Jagadish, C. *Nano Lett.* **2010,** 10, (3), 908-15.

(26) Lu, Z. Y.; Chen, P. P.; Liao, Z. M.; Shi, S. X.; Sun, Y.; Li, T. X.; Zhang, Y. H.; Zou, J.; Lu, W. *J. Alloys Compd.* **2013,** 580, 82-87.

(27) Ketterer, B.; Heiss, M.; Uccelli, E.; Arbiol, J.; i Morral, A. F. *ACS Nano* **2011,** 5, (9), 7585-92.

(28) Lu, Z. Y.; Shi, S. X.; Lu, J.; Chen, P. P. *J. Lumin.* **2014,** 152, 258-261.

(29) Wilson, T.; Hylton, N. P.; Harada, Y.; Pearce, P.; Alonso-Alvarez, D.; Mellor, A.; Richards, R. D.; David, J. P. R.; Ekins-Daukes, N. J. *Sci Rep* **2018,** 8, (1), 6457.

(30) Furthmeier, S.; Dirnberger, F.; Hubmann, J.; Bauer, B.; Korn, T.; Schüller, C.; Zweck, J.; Reiger, E.; Bougeard, D. *Appl. Phys. Lett.* **2014,** 105, (22), 222109.

(31) Alberi, K.; Wu, J.; Walukiewicz, W.; Yu, K. M.; Dubon, O. D.; Watkins, S. P.; Wang, C. X.; Liu, X.; Cho, Y. J.; Furdyna, J. *Phys. Rev. B* **2007,** 75, (4), 045203.

(32) Zhang, B.; Qiu, W. Y.; Chen, P. P.; Wang, X. J. *J. Appl. Phys.* **2018,** 123, (3), 035702.

(33) Vainorius, N.; Kubitza, S.; Lehmann, S.; Samuelson, L.; Dick, K. A.; Pistol, M. E. *Nanoscale* **2018,** 10, (3), 1481-1486.

(34) Trommer, R.; Cardona, M. *Phys. Rev. B* **1978,** 17, (4), 1865-1876.

(35) Kauschke, W.; Cardona, M.; Bauser, E. *Phys. Rev. B* **1987,** 35, (15), 8030-8041.

(36) Ketterer, B.; Heiss, M.; Livrozet, M. J.; Rudolph, A.; Reiger, E.; Morral, A. F. I. *Phys. Rev. B* **2011,** 83, (12), 125307.

(37) Habchi, M. M.; Ben Nasr, A.; Rebey, A.; El Jani, B. *Infrared Phys Techn* **2014,** 67, 531-536.

(38) Gladysiewicz, M.; Kudrawiec, R.; Wartak, M. S. *J. Appl. Phys.* **2015,** 118, (5), 055702.

(39) Heiss, M.; Conesa-Boj, S.; Ren, J.; Tseng, H. H.; Gali, A.; Rudolph, A.; Uccelli, E.;

Peiro, F.; Morante, J. R.; Schuh, D.; Reiger, E.; Kaxiras, E.; Arbiol, J.; Morral, A. F. I. *Phys. Rev. B* **2011,** 83, (4), 045303.

(40) Adler, S. L. *Phys. Rev.* **1962,** 126, (1), 118-122.

(41) Chuang, S. L.; Chang, C. S. *Phys. Rev. B* **1996,** 54, (4), 2491-2504.

(42) Buyanova, I. A.; Chen, W. M.; Tu, C. W. *Semicond. Sci. Technol.* **2002,** 17, (8), 815-822.

(43) Mohmad, A. R.; Bastiman, F.; Hunter, C. J.; Richards, R. D.; Sweeney, S. J.; Ng, J. S.; David, J. P. R.; Majlis, B. Y. *Phys. Status Solidi B* **2014,** 251, (6), 1276-1281.

(44) Tran, T. K.; Park, W.; Tong, W.; Kyi, M. M.; Wagner, B. K.; Summers, C. J. *J. Appl. Phys.* **1997,** 81, (6), 2803-2809.

(45) Lu, X.; Beaton, D. A.; Lewis, R. B.; Tiedje, T.; Whitwick, M. B. *Appl. Phys. Lett.* **2008,** 92, (19), 192110.

Figure captions

Figure 1. TEM micrographs of representative GaBiAs NW (a) and GaAs NW (b) with a scale bar of 200 nm. The regions of the nanowires marked by the green and red lines indicate the predominant 2H and 4H crystal structure in these parts of the nanowires, respectively. The lower panels of (a) and (b) show high-magnification images of the areas of the nanowires, together with fast Fourier transform (FFT) patterns. The scale bars in the insets are 5 nm.

Figure 2. (a) Schematic drawing of the experimental configuration for polarized PL and PLE spectra in a back-scattering geometry. The nanowire axis is along the z axis, and the incident and back-scattered laser light propagate along the x axis perpendicular to the substrate plane and the z axis. (b) Schematic illustration of the allowed optical transitions and their polarization directions in wurtzite Ga(Bi)As involving the topmost three valence subbands (with symmetry Γ_9, Γ_7 and Γ_7, respectively) and the lowest conduction band (symmetry Γ_7). The single (double) arrows represent transitions detected in PLE (PL and PLE) spectra. (c) and (d) Polarization-resolved PL and PLE spectra measured at T= 5K from individual wurtzite GaAs and GaBiAs NWs. The orange (violet) solid lines show the PL spectra detected in PL polarization parallel (perpendicular) to the NW axis, while the red (blue) symbols represents the PLE spectra under the light excitation with linear polarization parallel (perpendicular) to the NW axis. The vertical dashed line marks the detection energy monitored in the PLE measurements of each NW.

Figure 3. (a) Schematic diagram illustrating temperature dependences of the A- B- and C-optical transitions. The horizontal solid lines labeled as "Laser" represents the excitation laser energy $\hbar\omega_i$, whereas the wavy arrow illustrates emission of the LO phonon with the energy $\hbar\omega_{LO}$. The condition for an outgoing Raman resonance with the $\Gamma_7(C) - \Gamma_7(CB)$ transition is met when $E_C^{GaBiAs} = \hbar\omega_s = \hbar\omega_i - \hbar\omega_{LO}$ at $T_{Resonance}$. (b) LO-phonon resonance profiles I_{LO}/I_{TO} for GaAs (cyan filled squares) and GaBiAs nanowires (orange filled circles). The

resonance temperature of the GaBiAs NW is extracted by fitting the resonance profile with a Gaussian function. The inset shows the Raman spectra of the GaBiAs NW at T=90 K (red) and room temperature (black).

Figure 4. (a) Schematic illustration of the valence band structure of ZB and WZ GaAs, as well as WZ GaBiAs, at the Γ point of the Brillouin zone. The Bi levels in ZB and WZ GaAs are assumed to be constant relative to the vacuum level. (b) The valence band structure of WZ GaBiAs as a function of the hybridization energy $V_{X,Y}$. The vertical dashed arrows relate interacting Bi states and host valence band states, accompanied by the corresponding matrix elements of hybridization terms in the perturbation Hamiltonian.

Figure 5. The peak energy of the PL emission from GaAs (cyan filled squares) and GaBiAs NW(red filled circles) as a function of temperature. The solid lines are expected temperature dependence of band-gap energy by a modified Varshni's equation. The band-gap reduction of the GaBiAs NW exhibits a significantly slower trend.

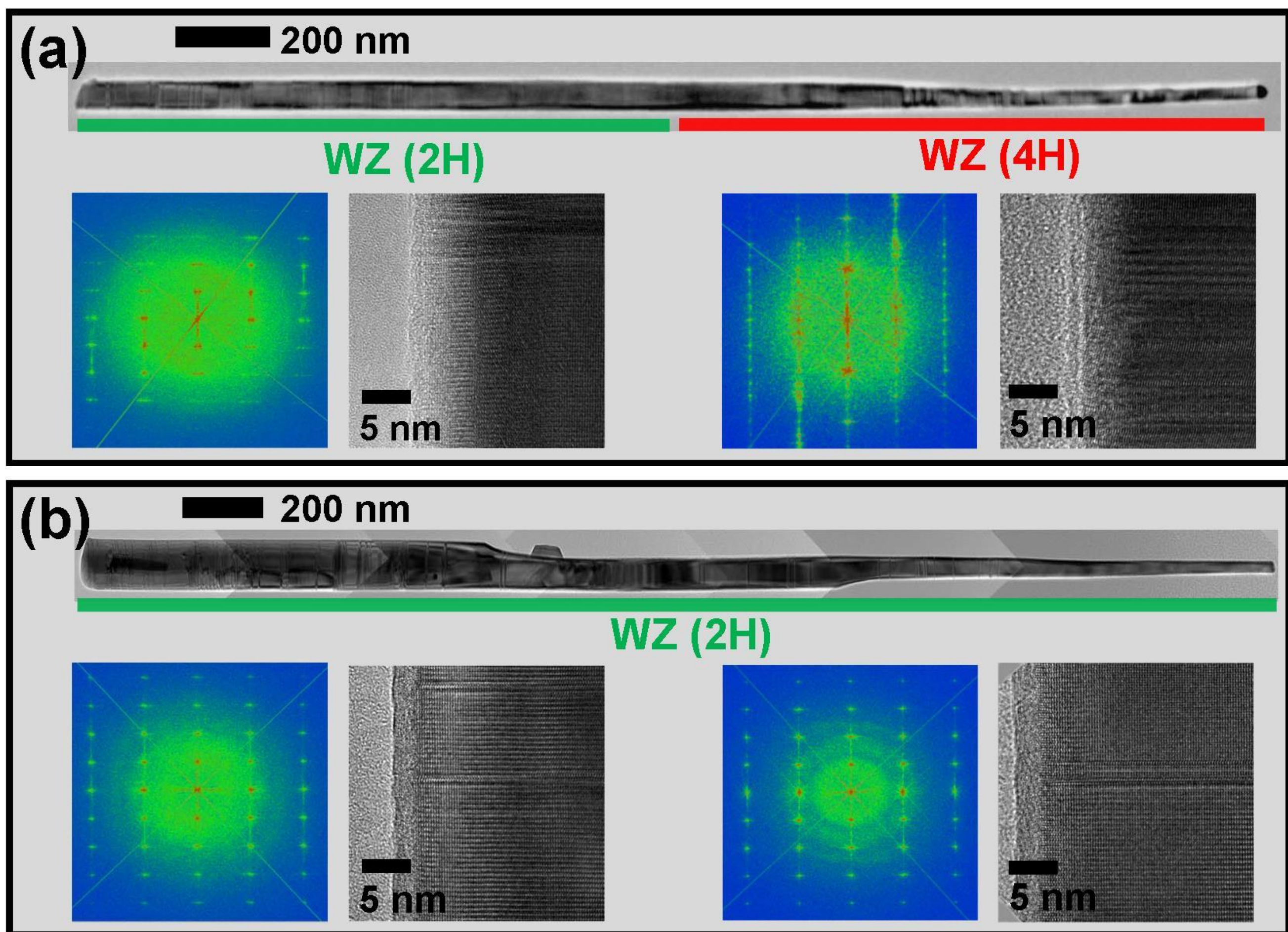

Fig. 1

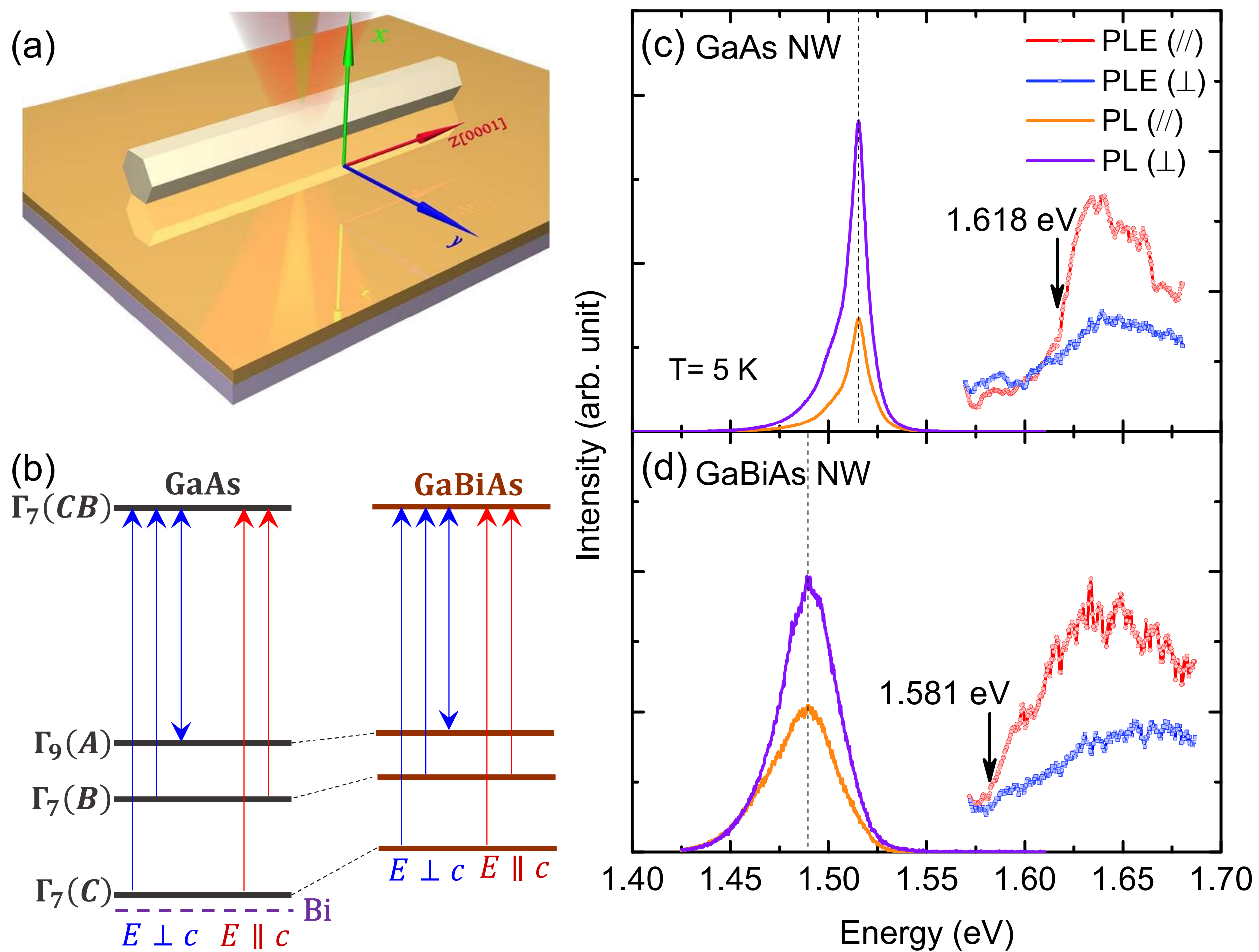

Fig. 2

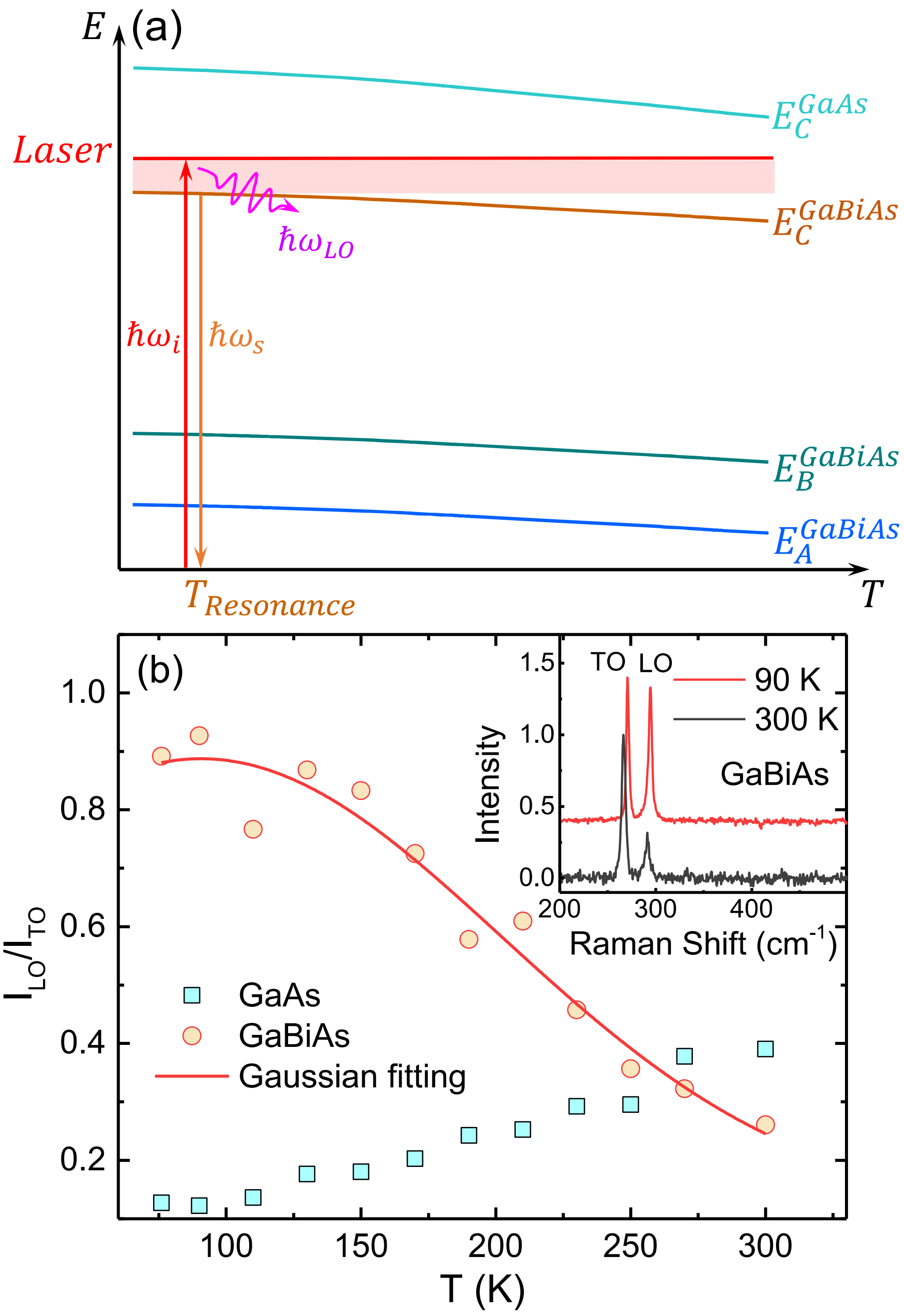

Fig. 3

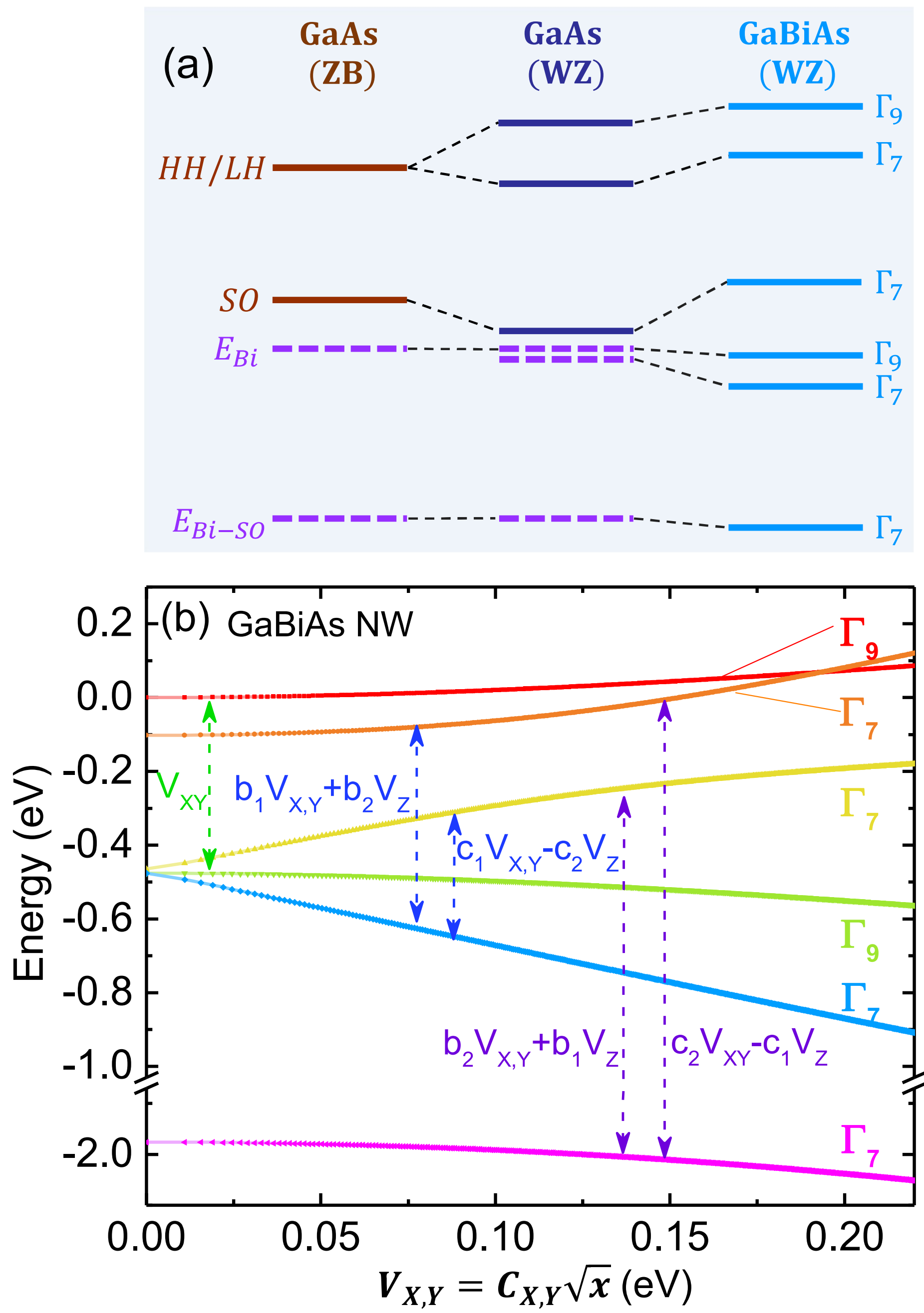

Fig. 4

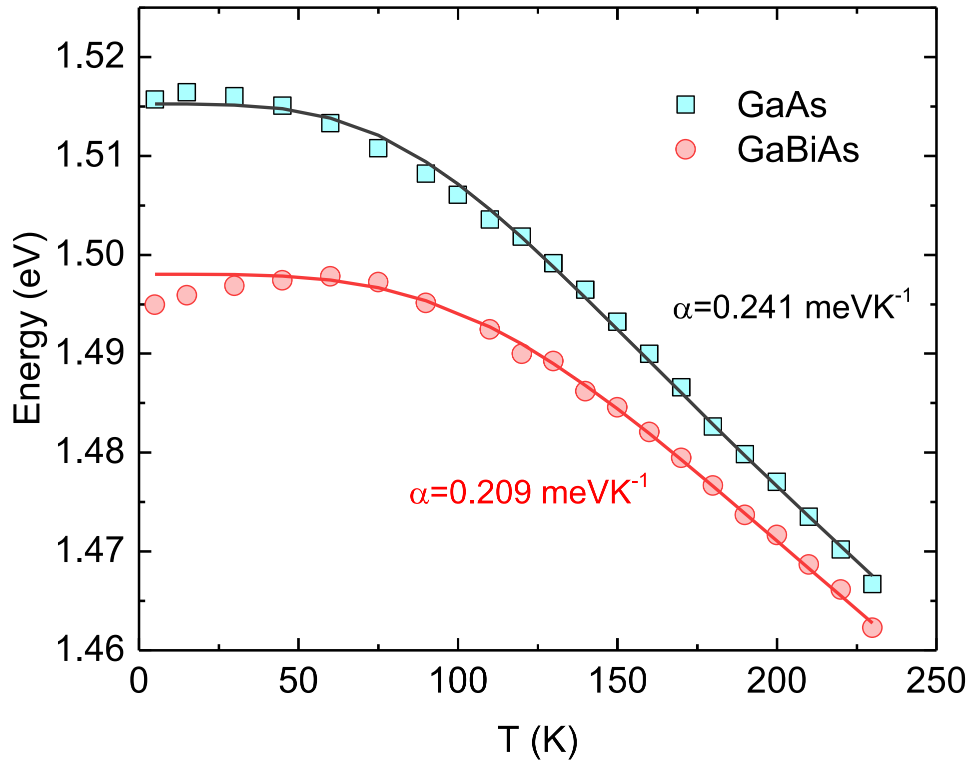

Fig. 5